Submitted to International Journal of Refrigeration, memorial issue of Professor Koyama

Title

Feasibility analysis for intermediated fluid type LNG vaporizers using R32 and R410A considering fluid properties

Authors:

Kosuke HIGASHI[(a)],

Chieko KONDOU[(b)*],

Shigeru KOYAMA[(c)]

Affiliations:

[(a)] Kobe Steel L.T.D., Kobe, 651-2271, Japan, higashi.kosuke@kobelco.com

[(b)]Nagasaki University, Nagasaki, 852-8521, Japan, ckondou@nagasaki-u.ac.jp

[(c)]Kyushu University, Fukuoka, 819-0395, Japan, koyama@cm.kyushu-u.ac.jp

* Corresponding author

Chieko Kondou, PhD

Professor, Nagasaki University

Graduate School of Engineering, Division of System Science

1-14 Bunkyo-machi Nagasaki 852-8521 Japan

+81 95 819 2527 / ckondou@nagasaki-u.ac.jp

Abstract

LNG vaporizer is widely used all over the world to vaporize LNG by using seawater. An intermediated fluid type vaporizer (IFV) uses intermediated fluid between LNG and heat source to transfer heat, and is enable to utilize LNG cold energy for a cryogenic power generation, and so on. Conventionally propane has been used as an intermediated fluid; however, refrigerants other than propane are recently needed because of the diversified usage environments. In this study, R32 and R410A are selected and their feasibility is discussed in heat transfer aspect. By using a number of unit (NTU) method, prediction of boiling and condensation heat transfer rate in tube bundles was carried out. The prediction demonstrated that those selected refrigerants can increase the vaporization rate with IFV from the base line of propane. From those, feasibility of refrigerant use in IFV was shown.

Keywords; refrigerant; heat transfer; tube bundles; LNG vaporizer

NOMENCLATURE

c	:specific heat of tube material in Eq. (2) [J kg^{-1}K^{-1}]
$C_{\min}$	:heat capacity flow rate of heat source or LNG [W K^{-1}]
c_p	:isobaric specific heat [J kg^{-1}K^{-1}]
D_b	:equilibrium breakoff bubble diameter [m]
D_i	:inner diameter of tube [m]
D_o	:outer diameter of tube [m]
$F_{p_{red}}$	:influence term of vapor pressure in Eq. (2) [-]
$F_{q_{wall}}$	:influence term of heat flux in Eq. (2) [-]
F_R	:influence term of tube surface roughness in Eq. (2) [-]
f_{wm}	:material constant in Eq. (3) [-]
F_{wm}	:material constant in Eq. (2) [-]
g	:gravitational acceleration [m s^{-2}]
Ga	:Galileo number [-]
Gr	:Grashof number [-]
h_{fg}	:latent heat of vaporization [J kg^{-1}]
h_i	:heat transfer coefficient inside of a tube [Wm^{-2}K^{-1}]
h_o	:heat transfer coefficient outside of a tube [Wm^{-2}K^{-1}]
Ja	:Jacob number [-]
K	:overall heat transfer coefficient [W m^{-2}K^{-1}]
M	:molar mass in Eq. (3) [g mol^{-1}]
m	:flow rate [kg s^{-1}]
m_{total}	: total condensate flow in Fig. 12
NTU	:number of transfer unit [-]
Nu	:Nusselt number [-]
p_l	:vertical tube pitch [m]
p_{red}	:reduced pressure [-]
p_t	:transverse tube pitch [m]
Q	:heat transfer rate [W]
q_{wall}	:heat flux outside of a tube [Wm^{-2}K^{-1}]
R_a	:arithmetic mean surface roughness in Eqs.(2) and (3) [μm]
Re	:Reynolds number [-]
Re_{fu}	:film Reynolds number in Eqs. (10) and (11) [-]
T_o	:tube outer surface temperature [K]
T_{sat}	:saturation temperature [K]

U_V	:vapor velocity across the minimum cross sectional area [m s^{-1}]
$(dp/dT)_{sat}$	:saturated vapor pressure curve [Pa K^{-1}]
ε	:effectiveness [-]
λ	:thermal conductivity [W $m^{-1}K^{-1}$]
μ	:viscosity [Pa·s]
ν	:kinetic viscosity [m^2 s^{-1}]
θ	:contact angle in Eq. (2) [deg]
ρ	:density [kg m^{-3}]
σ	:surface tension [N m^{-1}]

Subscript

0	:reference state
Cu	:copper
D	:outer diameter as a characteristic length
i	:inside
in	:inlet
L	:saturated liquid state
o	:outside
out	:outlet
tube	:tube
V	:saturated vapor state

Superscript

i	:*i* th segment in longitudinal direction
j	:*j* th tube in vertical direction

1. INTRODUCTION

Liquid natural gas (LNG) with small emissions of CO_2, NOx, and SOx is well known as a cleaner energy than coals and petroleum. Due to the recent increase in the interest to the global warming mitigation, the demand for LNG is notably increasing. In general, LNG is liquefied in producing countries, and transported mainly by tankers to demanding countries. The transported LNG is re-gasified by the LNG vaporizer and transported to consumption regions. Heat sources to vaporize LNG, such as sea water and industrially wasted water, are utilized for the re-gasification terminals. Table 1 shows popular LNG vaporizing systems currently used in LNG re-gasification terminals. Each vaporizer has features such as structure and heat source to be used, and an optimum vaporizer is adopted on the basis of operation plan of each terminal, LNG vaporization capacity, and conditions of heat sources (e.g., Petal et al., 2013; Astolfi et al., 2017). The LNG receiving terminals are all located in coastal areas to receive the transported LNG by tankers directly. Therefore, open rack vaporizer (ORV) and intermediate fluid type vaporizer (IFV), which can utilize abundant sea water as a heat source, are mainly adopted as vaporizers for base loads.

The intermediate fluid type LNG vaporizer, hereinafter referred to as IFV, is a vaporizer which uses an intermediate fluid between LNG and the heat source, and has the device configuration as shown in Figure 1. The intermediate fluid evaporates by being heated and absorbs heat from a heating source in the evaporator ("E-1" in Fig.1), while the heat of the intermediate fluid is transmitted to LNG by being cooled and condensed in the condenser ("E-2" in Fig. 1). During this, the intermediate fluids circulates by the gravitational force in the IFV system. IFV is mainly applied to the cases of using cold energy such as cold power generation (e.g., Atienza et al., 2019; Hadid and Zoughaib, 2017; Gao et al., 2011), intake air cooling, the case of using in dirty sea water areas, and so on (e.g., Lin et al., 2017). Propane has been conventionally used as an intermediate fluid of IFV. Xu et al. (2015) numerically assessed the feasibility of hydrocarbons: propylene, isobutane, butane and DME. However, since a large amount of intermediate fluid is charged in IFVs, less flammable refrigerants other than propane and such hydrocarbons are requested by diversification of recent use environments. Liu et al. (2013) proposed a titanium spiral wound tube heat exchanger to reduce charge amount. Han et al. (2018) assessed overall heat transfer coefficients of propane, propylene, butane, and DME and non-flammable refrigerants R134a, R22. The freezing points of R134a and R22 are -103 ºC (Di Nicola et al, 2012) and -160 ºC (Mc Linden, 1990), respectively. The freezing point of R134a is notably higher than LNG, while GWP of R22 is the ozone depleting substance regulated by the Montreal Protocol. In this study, R32 and R410A with a freezing point below -130 ºC were selected as the intermediate fluid alternative to propane. Although, both refrigerants are widely used for air conditioning, there is no case of understanding the performance when they are applied to vaporizers. Therefore, in this study, a calculation model to predict the vaporization performance of IFV is developed, and comparatively verified with experimental results using a laboratory scaled IFV system. The effects of rising bubbles

in evaporator and inundation in condenser are discussed with the calculated heat transfer coefficient distribution. From the results, the feasibility applying R32 and R410A in IFV was examined in the aspect of LNG vaporization performance.

Table 1 Various types of applied LNG vaporizer

Type	Open rack vaporizer (ORV)	Intermediate fluid type vaporizer (IFV)	Submerged combustion vaporizer (SCV)	Air fin type vaporizer (AFV)	Hot water type vaporizer (HWV)
Heat source	Seawater, River water, Warm discharged water, etc.	Seawater, River water, Warm discharged water, etc.	Fuel gas (e.g., Qi et al. 2016)	Atmospheric air	Hot water
Usage	Base load	Base load	Peak shaving, Emergency use	Satellite facility	Satellite facility, Emergency use
Capacity	Medium-Large	Medium-Large	Medium-Large	Small-Medium	Small-Medium
Feature	・LNG flows inside of a panel, while seawater flows outside of a panel.	・LNG is vaporized by intermediate fluid, then heated to a target temperature by seawater.	・LNG is vaporized by hot water which heated by submerged combustion burners.	・LNG is vaporized by natural or forced convection of air. ・Defog system is available.	・LNG is vaporized by hot water supplied from other system. ・Easy maintenance.
Operation	・LNG flow is controlled by send out demand. ・Simple operation.	・LNG flow is controlled by send out demand. ・Intermediate fluid is required.	・LNG flow and fuel gas for burner are controlled by send out demand.	・LNG flow is controlled by send out demand. ・Simplest operation. ・Defrost operation is required.	・Compact size for small capacity vaporizer.
Maintenance	・Visual inspection and cleaning for seawater distribution system. ・Inspection for thermal sprayed coating on panel.	・Visual inspection and cleaning for inside of heat source tubes.	・Inspection for blower working. ・Inspection for control system of fuel.	・Inspection for fan (applied for forced draft type).	・Inspection and cleaning for heating medium path.
Cost: Construction Running	 High Low	 High Low	 Low High	 Low Low	 Low High
Main materials	Aluminum alloy	Austenite stainless steel, Titanium alloy.	Austenite stainless steel.	Aluminum alloy.	Austenite stainless steel.

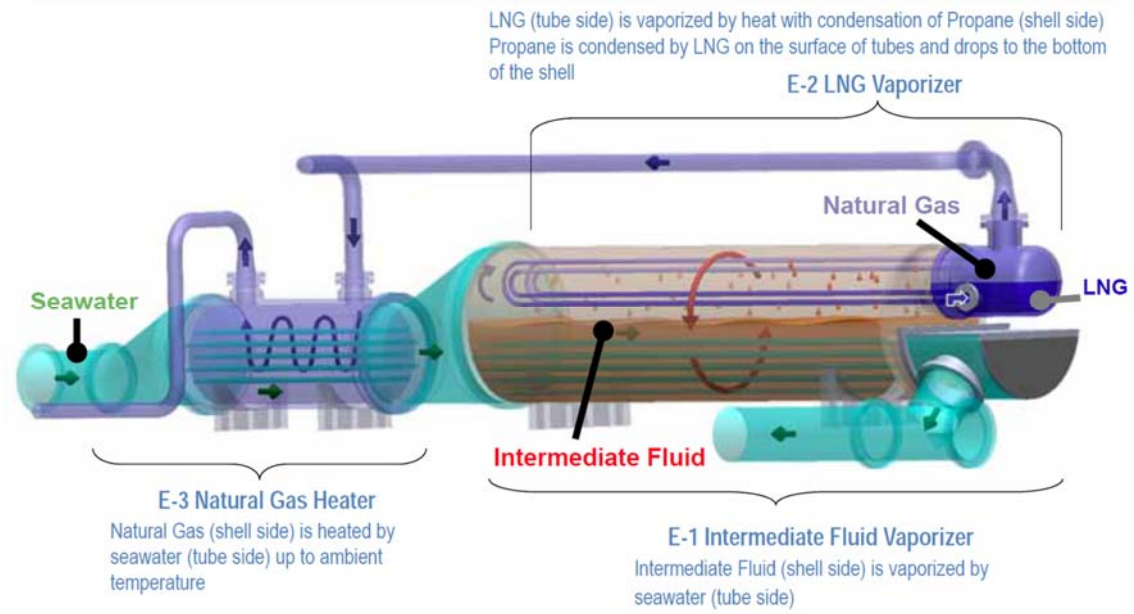

Fig. 1 Intermediated Fluid type LNG vaporizer

2. Selected refrigerants as the intermediate fluid

In the vaporizers, LNG is heated from -160 ºC to an ambient temperature. Thus, it is important to avoid circulation cessation of the intermediate fluid by freezing even at such low temperatures. It is also important that intermediate fluid has a sufficient latent heat and performs high heat transfer rate for a downsizing and a cost reduction. In addition, it is also necessary to consider their ozone depletion potential (ODP) and global warming potentials (GWP) complying the recent environmental regulations. As the intermediate fluid satisfies those conditions, two kinds of refrigerants which are used as refrigerants for air conditioning were nominated as candidate fluids. The physical properties of each refrigerant are compared to propane in Table 2. Those two refrigerants are examined in this study. The normal boiling points of R32 and R410A are comparable with that of propane; while the freezing points of R32 and R410A are higher. However, since the wall temperature of the condenser tube during heat exchange with LNG could go down to -100 ºC. Thus their freezing point is considered to be low enough to avoid solidification if the circulation flow rate is ensure. Additionally, ozone depletion potential and global warming potential must be low as much as possible. From above, R32 and R410 are selected to be calculated in the feasibility study.

Table 2 Propane (baseline) and selected refrigerant as the intermediate fluid

	Propane	R32	R410A R32/R125 (50/50mass%)
Chemical Type	Hydrocarbon	HFC	HFC blend
ODP [a)]	0	0	0
GWP [b)]	3	675	2090
Molar mass	44.1 g mol^{-1}	52.0 g mol^{-1}	72.6 g mol^{-1}
Normal boiling point	-42 ºC	-52 ºC	-51 ºC
Freezing point	-188 ºC [c)]	-136 ºC [e)]	-155 ºC
Latent heat at -7 °C [f)]	384 kJ kg^{-1}	326 kJ kg^{-1}	230 kJ kg^{-1}
Saturated pressure at 55 °C [f)]	1.9 MPa	3.4 MPa	3.3 MPa
Temperature glide	-	-	0.10 K

a) Ozone depletion potential, Myhre et al. (2013)

b) Global warming potential of 100-years-time-horizon, Myhre et al. (2013)

c) Reeves et al., (1964)

d) McLinden (1990)

e) Di Nicola et al. (2012)

f) Calculated by REFRPOP9.2 (Lemmon et al., 2013)

3. Heat transfer performance prediction of a single tube

The boiling and condensation performances of above selected refrigerants and propane are comparatively studied in order to discuss the applicability to IFV in heat transfer performance. First, a performance prediction model using a single tube was developed for each refrigerant, and then the heat transfer performance was relatively compared. Physical property calculation software REFPROP 9.2 (Lemmon et al., 2013) was used for each fluid property value used in the calculation. R410A is a mixed refrigerant of R32 and R125 with a temperature glide of only 0.1 K is treated as an azeotropic refrigerant for simplification.

3.1 Evaporation heat transfer

An outline of the evaporation performance prediction model on a single tube is shown in Fig. 2. In the model, assuming that a single tube is immersed in an intermediate fluid and the outside heat transfer state is nucleate boiling. The performance prediction was carried out by setting the saturation temperature in the shell to -7.0 ºC and the heat source (seawater) temperature to 9.6 ºC. To obtain heat transfer rate from LNG to the intermediate fluid, the boiling heat transfer coefficient of the intermediate fluid on the outside of the tube is predicted by the most authorized correlations.

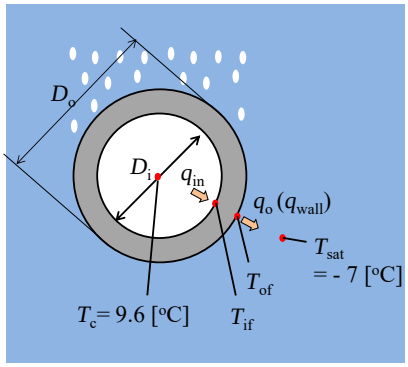

Fig. 2 Evaporation model on a single tube (Titanium)

Various empirical equations have been proposed for nucleate pool boiling heat transfer coefficient, and the calculation results vary depending on the applied system. Therefore, in this study, 4 predicting correlations were selected to calculate the pool boiling heat transfer coefficient of the intermediate fluids: propane as the baseline, R32 and R410A.

Stephan-Abdelsalam (1980) conducted a regression analysis of the pool boiling experiment data acquired by other researchers. Using several dimensionless numbers obtained from dimension analysis, they proposed a pool boiling correlation equations available for water, hydrocarbons, low-temperature fluids and refrigerants. The equation proposed for refrigerants Eq. (1) is selected.

$$Nu = \frac{h_o D_o}{\lambda_L} = 207 Pr_L^{0.533} \left(\frac{q_{wall} D_b}{\lambda_L T_{sat}} \right)^{0.745} \left(\frac{\rho_V}{\rho_L} \right)^{0.581}$$
$$D_b = 0.0146\theta \sqrt{\frac{2\sigma_L}{g(\rho_L - \rho_V)}}, \quad \theta = 35 \text{ deg for refrigerants} \tag{1}$$

where, h_o is the heat transfer coefficient on the tube outer surface in $Wm^{-2}K^{-1}$. λ_L, Pr_L, and ρ_L are thermal conductivity, Prandtl number, and density of the intermediate fluid at a saturated liquid state. ρv is density at a saturated vapor state. T_{sat} is the saturation temperature of intermediate fluid. The wall heat flux q_{wall} is implicitly obtained to satisfy the heat balance of inner and outer tube surfaces as later explained.

Gorenflo et al. (2010, 2014) acquired pool boiling experimental data of various refrigerants using brass, stainless and copper heat transfer tubes and proposed a correlation equation as a function of the wall heat flux, reduced pressure, refrigerant physical properties, and heat transfer surface properties on heat transfer characteristics of pool boiling. The following equation is the correlation of Gorenflo et al. (2010) used in this study.

$$\frac{h_{\mathrm{o}}}{h_{\mathrm{o},0}} = F_{q_{\mathrm{wall}}} F_{p_{\mathrm{red}}} F_R F_{wm}$$

$$h_{\mathrm{o},0} = 3580 \cdot P_f^{\,0.6},\ P_f = \left(\frac{dp}{dT}\right)_{\mathrm{sat}} \Big/ \sigma_{\mathrm{L}} \quad \text{at } p_{\mathrm{red}}=0.1$$

$$\begin{cases} F_{q_{\mathrm{wall}}} = \left(\dfrac{q_{\mathrm{wall}}}{q_{\mathrm{wall},0}}\right)^{0.95-0.3\,p_{\mathrm{red}}^{\,0.3}}, \quad q_{\mathrm{wall},0} = 20 \ \ \mathrm{kWm^{-2}} \\ F_{p_{\mathrm{red}}} = 0.7\,p_{\mathrm{red}}^{\,0.2} + 4\,p_{\mathrm{red}} + \dfrac{1.4\,p_{\mathrm{red}}}{(1-p_{\mathrm{red}})} \\ F_R = \left(\dfrac{R_a}{R_{a0}}\right)^{\frac{2}{15}}, \quad R_{a0} = 0.4 \ \ \mu\mathrm{m} \\ F_{\mathrm{wm}} = \left(\dfrac{\rho_{\mathrm{tube}} c_{\mathrm{tube}} \lambda_{\mathrm{tube}}}{\rho_{\mathrm{Cu}} c_{\mathrm{Cu}} \lambda_{\mathrm{Cu}}}\right)^{0.25}, \quad F_{\mathrm{wm}} = 1 \quad \text{for copper tube} \end{cases} \tag{2}$$

Ribatski-Jabardo (2003) conducted pool boiling experiments using copper, brass and stainless heat transfer tubes and proposed the following correlation for pool boiling heat transfer as a function of heat flux, reduced pressure, surface roughness, molar mass, and material constant.

$$h_{\mathrm{o}} = f_{\mathrm{wm}} q_{\mathrm{wall}}^{\,0.9-0.3\,p_{\mathrm{red}}^{\,0.2}} p_{\mathrm{red}}^{\,0.45} \left[-\log\left(p_{\mathrm{red}}\right)\right]^{-0.8} R_{\mathrm{a}}^{\,0.2} M^{-0.5}$$

$$\text{where, } f_{\mathrm{wm}} \begin{cases} 100 & \text{for copper} \\ 110 & \text{for brass} \\ 85 & \text{for stainless steel} \end{cases} \tag{3}$$

Nagata et al. (2017) determined the material constant 90.6 for titanium tubes with outer diameters from 18.66 to 19.12 mm based on their experiment using R1234ze(Z) . In this study, the material constant f_{wm} and the roughness R_{a} were set to 90.6 and 0.5 μm.

Jung et al. (2003) conducted pool boiling experiments of HFC refrigerants on copper smooth tubes by reference to pool boiling heat transfer correlation equations of Stephan-Abdelsalam (1980) and Cooper (1984) and proposed a pool boiling heat transfer correlation, as shown below.

$$h_{\mathrm{o}} = 10 \frac{\lambda_{\mathrm{L}}}{D_{\mathrm{b}}} \left[\frac{q_{\mathrm{wall}} D_{\mathrm{b}}}{\lambda_{\mathrm{L}} T_{\mathrm{sat}}}\right]^{C_1} p_{\mathrm{red}}^{\,0.1} \left(1-T_{\mathrm{red}}\right)^{-1.4} Pr_{\mathrm{L}}^{\,-0.25}$$

$$C_1 = 0.855 \left(\frac{\rho_{\mathrm{V}}}{\rho_{\mathrm{L}}}\right)^{0.309} p_{\mathrm{red}}^{\,-0.437}, \quad D_{\mathrm{b}} = 0.0146\theta \sqrt{\frac{2\sigma_{\mathrm{L}}}{g\left(\rho_{\mathrm{L}} - \rho_{\mathrm{V}}\right)}} \tag{4}$$

On the other hand, the heat transfer coefficient in the tube corresponding to the heat transfer of the

heating source side (sea water) was obtained from a Dittus-Boelter equation, Eq. (5). This is the most common equation available for fully developed single phase flow in long circular tubes.

$$Nu = \frac{h_i D_i}{\lambda} = 0.023 Re_{D_i}{}^{0.8} Pr^n \tag{5}$$

where $n = 0.4$ for heating mode and $n = 0.3$ for cooling mode. The fluid properties of heating source are represented by water for simplification. The typical Reynolds number Re_{D_i} is approximately 28950 in the actual system.

The overall heat transfer coefficient, K, based on outside tube surface area is calculated using Eq. (6).

$$K = \frac{1}{h_{\mathrm{i}}\left(\frac{D_{\mathrm{o}}}{D_{\mathrm{i}}}\right)} + \frac{D_{\mathrm{o}}}{2\lambda_{\mathrm{tube}}} \ln\left(\frac{D_{\mathrm{o}}}{D_{\mathrm{i}}}\right) + \frac{1}{h_{\mathrm{o}}} \tag{6}$$

The calculation procedure is specified in Fig. 3. First, the internal heat transfer coefficient h_{i} is calculated by Eq. (5). Then, temporarily determined heat flux, q_{o}, was given and the pool boiling heat transfer coefficient h_{o} is calculated by one of the predicting correlation. From those heat transfer coefficients, the outside and inside tube wall temperatures were calculated. Using these temperatures and heat transfer coefficients, the heat flux is re-calculated and assigned a symbol, $q_{\mathrm{o}}{}'$. With this new heat flux the pool boiling heat transfer coefficient and tube wall temperatures are calculated. The repeated calculation is carried out until re-calculated heat flux, $q_{\mathrm{o}}{}'$, becomes the same value of the prior, q_{o}.

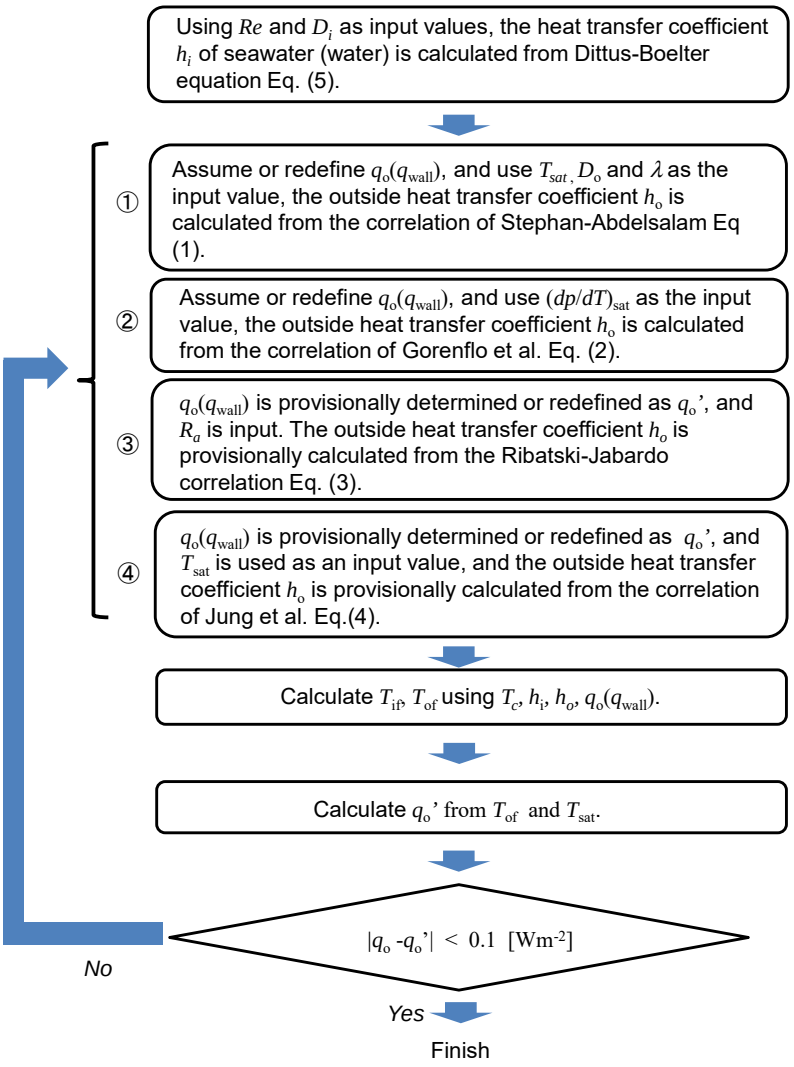

Fig. 3 Evaporation calculation flow on a single tube

3.2 Condensation heat transfer

Fig. 4 shows the heat transfer prediction model of a single tube for condensation. In this model, LNG flows in the tube and the heat transfer mode of intermediate fluid side on the tube is assumed as film wise condensation. Nusselt equation (1916) is the most authorize theoretical correlation of free convective filmwise condensation on a single horizontal smooth circular tube. This is shown in Eq. (7).

$$Nu = \frac{h_o D_o}{\lambda_L} = 0.728\left(\frac{GaPr_L}{Ja}\right)^{\frac{1}{4}}$$
$$Ga = \frac{gD_o^{\,3}}{\nu_L^{\,2}}\left(\frac{\rho_L - \rho_V}{\rho_L}\right), \quad Ja = \frac{c_{pL}\left(T_{sat} - T_o\right)}{h_{fg}} \tag{7}$$

The saturation temperature in the shell, T_{sat}, was set to -7.0 ºC; meanwhile, the outside tube wall temperature, T_o, was set to -80 ºC that is an average value of LNG inlet temperature (-160 ºC) and LNG outlet temperature (0 ºC) for the comparison on condensation performance among the selected intermediate fluids.

On the other hand, the heat transfer coefficient in the tube is obtained from Dittus-Boelter Equation, Eq. (5). The Reynolds number Re_{Di} of LNG flow was set to 177300, referring to typical operation conditions. The overall heat transfer coefficient is calculated by using Eq. (6). The above calculation flow is specified in Fig. 5.

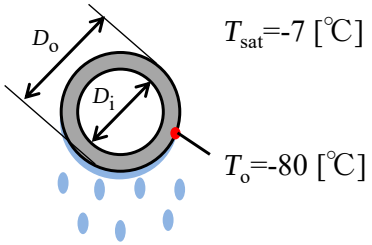

Fig. 4 Condensation model of a single tube (Stainless)

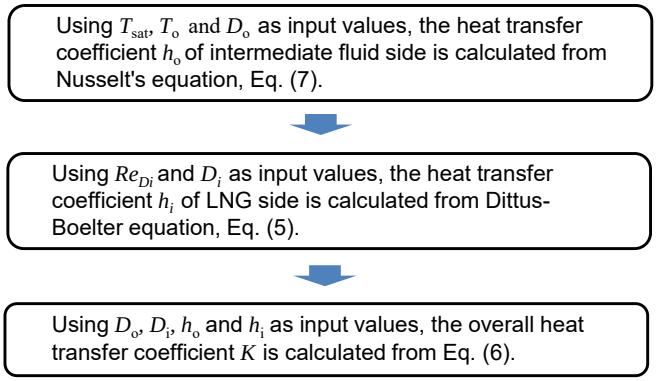

Fig. 5 Condensation calculation flow on a single tube

3.3 Experimental evaluation on heat transfer performance of a single tube

Fig. 6 shows the prediction results on condensation and evaporation heat transfer performance of a

single tube. The bars show the overall heat transfer coefficients relative to the propane those are calculated by the correlations noted in the legend. It was clarified that the condensation performance calculated by Nusselt equation was improved by approximately 32% in R32 and approximately 11% in R410A to propane. On the other hand, the relative merits and demerits of the evaporation performance changed depending on the prediction equation used. The correlations of Stephan-Abdelsalam (1980) and Ribatski-Jabardo (2003) underestimate the evaporation performance than propane; on the other hand, the correlations of Gorenflo et al. (2010) and Jung et al. (2003) overestimate the evaporation performance than propane.

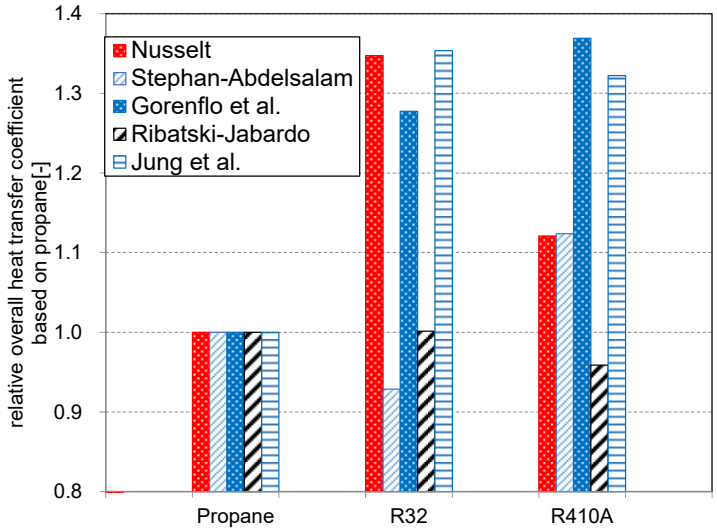

Fig. 6 Predicted overall heat transfer coefficients on a single tube. (relative overall heat transfer coefficient using Nusselt Eq. (7) for condensation heat transfer coefficient; Stephan-Abdelsalam Eq. (1), Gorenflo et al., Eq.(2), Ribatski-Jabardo Eq.(3), and Jung et al., Eq. (4) for pool boiling heat transfer coefficient)

In order to confirm the validity of this prediction method and obtained heat transfer performance, heat transfer experiments using the selected intermediate fluids were carried out with a laboratory scale IFV system using cold water as a cooling source and warm water as a heating source. An outline of the laboratory scale IFV system is shown in Fig. 7. The shell length and inner diameter are 1000 mm and 165 mm for both condenser and evaporator. Inside the condenser shell, 9 U-tunes of 15.9 mm outer diameter and 12.7 mm inner diameter are installed in staggered manner with a tube pitch of 22 mm. Inside of the evaporator, 4 straight tubes of 19.05 mm and 16.65 mm are installed in staggered manner with a tube pitch of 60 mm. The temperature of cold water was controlled using a chiller, and

that of warm water was controlled using an electric heater. The tested intermediate fluid is circulated between the cooling source and the heating source by thermosiphon, in a manner same as IFV. The transfer rate is determined from the heat balance of cooling and heating water sides: inlet and outlet temperatures and flow rates. Meanwhile, the heat transfer coefficient on the outside of the tube is determined from outer surface temperature of the tube and saturation temperature of the intermediate fluid that is determined from the measured pressure. The experimental conditions are listed in Table 3. Table 4 lists the uncertainty in each measurement parameter and the uncertainty propagated in heat transfer rate at 2.5 kW and heat transfer coefficients. The most dominant factor in the propagated uncertainties is uncertainty in water temperatures. As the results, the uncertainty in boiling heat transfer coefficient exhibited 14%.

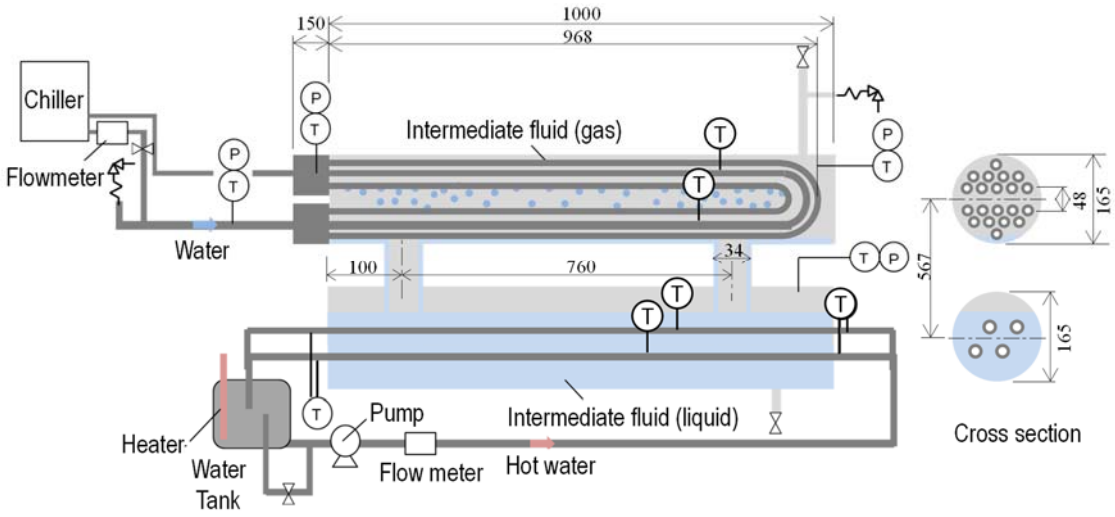

Fig. 7 Tested laboratory scale IFV system.

Fig. 8 shows the experimentally obtained heat transfer coefficient of pool boiling and condensation, and also the heat transfer rate relative to propane. As shown with red and gray bars in Fig. 8, the both boiling and condensation heat transfer coefficients of refrigerants obviously exceed that of propane. The heat transfer rate, plotted with the green line, thus increases approximately by 50% in R32 and approximately by 35% in R410A. These experimental results indicate that the application of R32 and R410A may provide higher heat transfer performance than propane. Comparing Fig. 8 with Fig. 6, the predicting method can be evaluated with the experimental results. For the condensation heat transfer, it was confirmed that Nusselt‘s equation shows a qualitative tendency in condensation. Among the selected predicting correlation for pool boiling heat transfer coefficient, the correlation of Jung et al. (2003) appears to be showing a qualitative tendency best. This is considered to be due to the fact that the boiling heat transfer rate of smooth tubes was corrected in the direction suitable for this system

using the low-temperature fluid by reference to Stephan-Abdelsalam's correlation (1980) referring to test results of low-temperature fluid.

As shown with a green line in Fig. 8, R32 exhibited the largest heat transfer rate. This is because, under the running pressure condition, the heat transfer coefficients for both condensation and evaporation are notably higher than the others, due to the favorable thermophysical properties: greater liquid thermal conductivity, smaller surface tension, and so on. Because the heat transfer area are fixed in the experimental setup, this means larger heat transfer rate. Moreover, R32 vapor is denser than the others and pressured drop is kept smaller during the circulation. Then the smooth circulation is kept at higher heat transfer rates (higher circulation rates) with the gravitational force.

Table 3 Experimental conditions

Cooling water	Inlet temperature [ºC]	5.0
	Volumetric flow rate [L min^{-1}]	5.0
Heating water	Inlet temperature [ºC]	26.0
	Volumetric flow rate [L min^{-1}]	30.0

Table 4 Measurement uncertainties and estimated propagated uncertainty of 95% confidence at a typical test condition

Parameters	**Instrument**	**Uncertainty (k =2)**
Cooling water flow rate	Volumetric flow meter	1.5% (0.08 L min^{-1})
Heating water flow rate	Volumetric flow meter	1.6% (0.45 L min^{-1})
Pressure of intermediate fluid	Pressure transducer	0.5% (0.2 K in T_{sat})
Temperature	Thermocouples calibrated with ITS-90	0.5 K
Propagated uncertainty in heat transfer rate at 2.5 kW		0.06 kW (condenser) 0.36 kW (evaporator)
Propagated uncertainty in heat transfer coefficient		2.4% (condenser) 14% (evaporator)

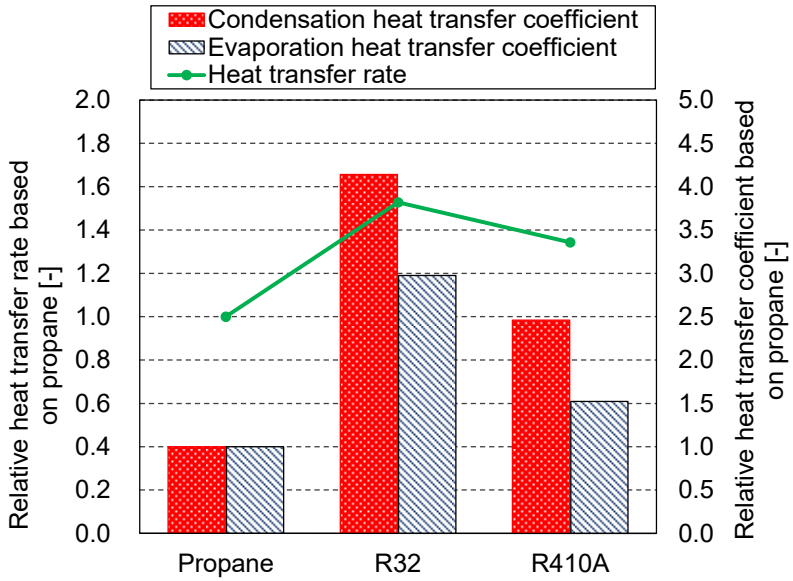

Fig. 8 Experimentally determined heat transfer performance for the selected intermediate fluids.

4. Simulation model of tube bundles to evaluate vaporization performance

Evaporator and condenser of actual IFV are composed of tube bundles. The heat transfer performance of tube bundles sometimes behaves unexpectedly different from that of single tubes. Thus, a performance prediction model is developed with the number of transfer units method for the tube bundles in evaporator and condenser, and then the vaporization performance is evaluated for the selected intermediate fluids.

4.1 Evaporator model

Fig. 9 shows a configuration of the tube bundles of the IFV evaporator. The tubes are arranged in a staggered arrangement in the cross section, and the column numbers are assigned vertically. In the longitudinal direction, i.e. flow direction of the heat source (sea water), the tube bundles of evaporator are divided into 8 segments.

As illustrated in Fig. 9, generated bubbles of the intermediate fluid rise in tube bundles. Due to the convective effect of the bubble motion, the boiling heat transfer coefficient on tube bundles can increase. The boiling heat transfer rate in tube bundles was calculated using the following empirical correlation of Ribatski et al. (2008).

$$\frac{h^N}{h^{N=1}} = 1 + 0.345 C_A p_{red}^{-1.4} q^{-1} \exp\left\{ -0.37 p_{red}^{-0.4} \left[\ln\left(\frac{q}{C_q p_{red}^{-0.7}} \right) \right]^2 \right\}$$

$$C_A = 160 - 85.2 \cdot \exp(-0.3N) \tag{8}$$

$$C_q = 63 + 1200 \cdot \exp(-0.3N)$$

where, N is a number of tube array in vertical direction from the bottom. $h^{N=1}$ is the reference heat transfer coefficient of the first bottom tube calculated by the correlation of Jung et al. (2003); while, h^N is that of the N th tube. This number of columns are set to 9 (i =18) in this study.

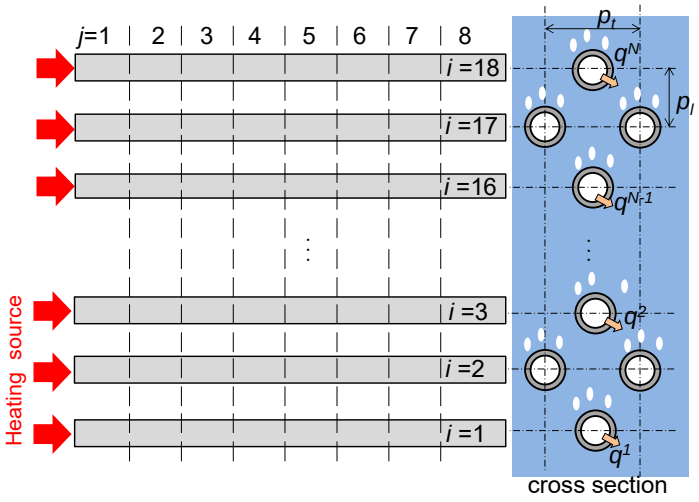

Fig. 9 Segmented calculation model of tube bundle IFV evaporator

Meanwhile, the heat transfer coefficient of the heat source (sea water) flowing in the tubes was calculated using Dittus-Boelter equation, Eq. (5). From those, the overall heat transfer coefficient in a segment of i th and j th in vertical and longitudinal directions, $K^{i,j}$, is calculated. The heat transfer rate in a segment, $\Delta Q^{i,j}$, is obtained using the number of transfer units method "ε-NTU" as shown in Eq. (9) in consideration of the calculation stability.

$$\Delta Q^{i,j} = \varepsilon^{i,j} C_{\min} \left(T_{\text{water,in}}{}^{i,j} - T_{\text{sat}} \right)$$

$$\varepsilon^{i,j} = 1 - \exp\left(-NTU^{i,j} \right)$$

$$NTU^{i,j} = \frac{K^{i,j} A}{C_{\min}} \tag{9}$$

$$C_{\min} = \left(mc_p \right)_{\text{water}}$$

where $C_{\min}$ is the heat capacity flow of water (heating source) in this case. A is a heat transfer area in

a segment. T_{sat} and $T_{water,in}^{i,j}$ are saturation temperatures of intermediate fluid and heat source inlet temperature of a segment, respectively. $\varepsilon^{i,j}$ and $NTU^{i,j}$ are an effectiveness and a number of transfer units in a segment, respectively.

Fig. 10 shows the calculation procedure of total heat transfer rate in evaporator. The outlet temperature of the heat transfer tube of a whole unit $T_{water,out}^{j}$ was assumed, then the total heat transfer rate Q_1^j can be defined. The heat flux in a segment is obtained, then the internal and external heat transfer coefficients, and the overall heat transfer coefficient $K^{i,j}$ are calculated. From Eq. (9), the heat transfer rate $\Delta Q^{i,j}$ in a segment is obtained, and then the heat source outlet temperature is sequentially obtained through a unit tube. The total heat transfer rate is re-defined as Q_2^j. Those are repeated until the difference between prior and current heat transfer rates becomes negligibly small. The above calculation is repeated for all heat transfer tubes and finally the total heat transfer rate in the evaporator is obtained.

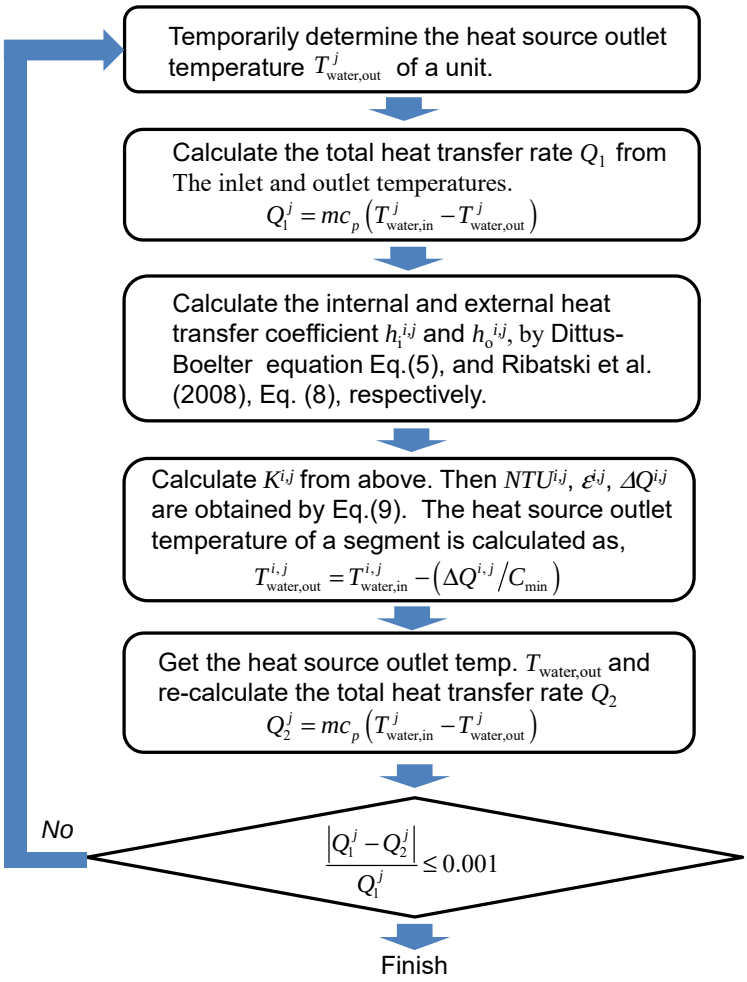

Fig. 10 Calculation procedure for evaporator

4.2 Condenser model

Fig. 11 illustrates the configuration of tube bundles in the IFV condenser. In the condenser, the U tubes are arranged in staggered arrangement in vertical direction. The tube bundles including outgoing and return tubes were divided into 26 in the flow direction of the LNG for heat transfer rate prediction.

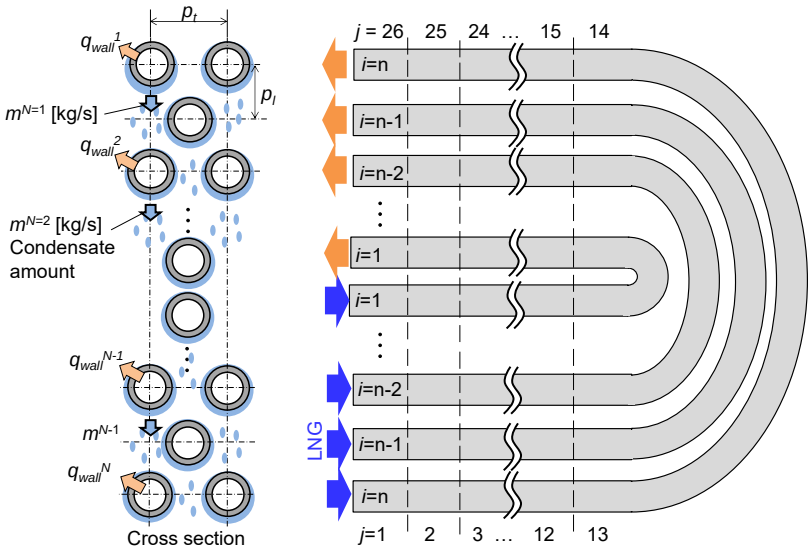

Fig. 11 Segmented calculation model of IFV condenser

The condensed liquid flows down dripping on the tube surfaces in the vertical downward. Thickening the liquid film covers the tube surfaces, and this resists the heat transfer and decreases condensation heat transfer coefficient. On the other hand, due to the convective effect of the liquid flow and drugged vapor flow, condensation heat transfer coefficient can increase in lower part of tube bundles. The complex condensation in tube bundles was calculated by the following correlation proposed by Honda et al. (1988).

$$
\begin{aligned}
&Nu_D = \left\{ {Nu_{Dg}}^4 + \left(Nu_{Dg} Nu_{Df} \right)^2 + {Nu_{Df}}^4 \right\}^{1/4} \\
&\begin{cases}
Nu_{Dg} = {Gr_D}^{1/3} \left\{ \left(1.2 / {Re_{fg}}^{0.3} \right)^4 + \left(0.072 {Re_{fg}}^{0.2} \right)^4 \right\}^{1/4} \\
Nu_{Df} = 0.165 \left(\dfrac{p_t}{p_l} \right)^{0.7} \left\{ {Re_{\mathrm{VD}}}^{-0.4} + 1.83 \left(\dfrac{{q_{\mathrm{wall}}}^N}{\rho_{\mathrm{V}} h_{fg} {U_{\mathrm{V}}}^N} \right) \right\}^{1/2} \left(\dfrac{\rho_{\mathrm{V}}}{\rho_{\mathrm{L}}} \right)^{1/2} \dfrac{{Re_{\mathrm{LD}}} {Pr_{\mathrm{L}}}^{0.4}}{{Re_{fu}}^{0.2}}
\end{cases}
\end{aligned}
\tag{10}
$$

Nu_{Dg} represents a convective heat transfer contribution of condensate flow driven by the gravity, and Nu_{Df} represents the contribution of that the condensate is uniformly dispersed by the inertia force of vapor speed. p_t and p_l are tube pitch in transverse and vertical directions. ${q_{\mathrm{wall}}}^N$ and ${U_{\mathrm{V}}}^N$ are the heat flux and vapor velocity across the minimum passage area between tubes of N th column. The non-dimensional parameters in Eq. (10) are defined as,

$$
\begin{aligned}
&{Re_{\mathrm{LD}}} = \frac{{U_{\mathrm{V}}}^N D_{\mathrm{o}}}{\nu_{\mathrm{L}}}, \quad {Re_{\mathrm{VD}}} = \frac{{U_{\mathrm{V}}}^N D_{\mathrm{o}}}{\nu_{\mathrm{V}}}, \quad {Gr_D} = \frac{g \rho_{\mathrm{L}} \left(\rho_{\mathrm{L}} - \rho_{\mathrm{V}} \right) {D_{\mathrm{o}}}^3}{{\mu_{\mathrm{L}}}^2} \\
&{Re_{fu}} = \begin{cases}
\dfrac{2\pi D_{\mathrm{o}} {q_{\mathrm{wall}}}^{N=1}}{\mu_{\mathrm{L}} h_{fg}} & (N = 1) \\
\dfrac{2\pi D_{\mathrm{o}}}{\mu_{\mathrm{L}} h_{fg}} \left(\displaystyle\sum_{k=1}^{N-1} {q_{\mathrm{wall}}}^k \frac{D_o}{p_t} + {q_{\mathrm{wall}}}^N \right) & (N > 2)
\end{cases}
\end{aligned}
\tag{11}
$$

The LNG heat transfer rate in the heat transfer tube was calculated using Dittus-Boelter equation of Eq. (5) with the physical properties of LNG represented by methane. At a near pseudo critical point, the boiling like flow (i.e., Shiralkar and Griffith, 1969) sometimes exhibits heat transfer degradation because of the phenomena similar to dryout or drypatch in flow boiling (i.e., Lei et al., 2013; Yamagata et al., 1972). Nevertheless the portion of enthalpy change under such heat transfer degradation in the total enthalpy change during LNG vaporization is quite small (Pu et al., 2014), and the change in LNG chemical composition considerably affects the heat transfer coefficient (Xu et al., 2018). In order to avoid the calculation divergence, using Eq. (5) is justified.

Fig. 12 shows the calculation flow of tube bundles in condenser. The heat transfer rate was obtained using ε-NTU method as well as the evaporator, however the heat capacity flow of LNG side is used in this case.

$$\Delta Q^{i,j} = \varepsilon^{i,j} C_{\min} \left(T_{\text{sat}} - T_{\text{LNG,in}}{}^{i,j} \right)$$
$$\varepsilon^{i,j} = 1 - \exp\left(-NTU^{i,j} \right) \tag{12}$$
$$NTU^{i,j} = \frac{K^{i,j} A}{C_{\min}}, \quad C_{\min} = \left(mc_p \right)_{\text{LNG}}$$

First, the LNG outlet temperature of the heat transfer tube of the unit $T^{j}_{\text{LNG,out}}$ and the condensate quantity in the return tube were once assumed without consideration of inundation. Then, the heat transfer rate $Q_1{}^{j}$ can be obtained from the inlet and outlet temperatures of a unit tube from Eq. (12). With the obtained heat flux, the overall heat transfer coefficient $K^{i,j}$, effectiveness $\varepsilon^{i,j}$, and heat transfer rate $\Delta Q^{i,j}$ in a segment are calculated. From this sequential calculation, the temperature distribution of LNG flow in a unit tube is calculated to satisfy the heat balance. The vapor velocity, U_{V}, and condensate flow rate from the whole tube bundle m_{total} is obtained and the above procedure is repeated with consideration of inundation next. Then change in the condensate flow rate is checked and repeatedly calculated until it converges.

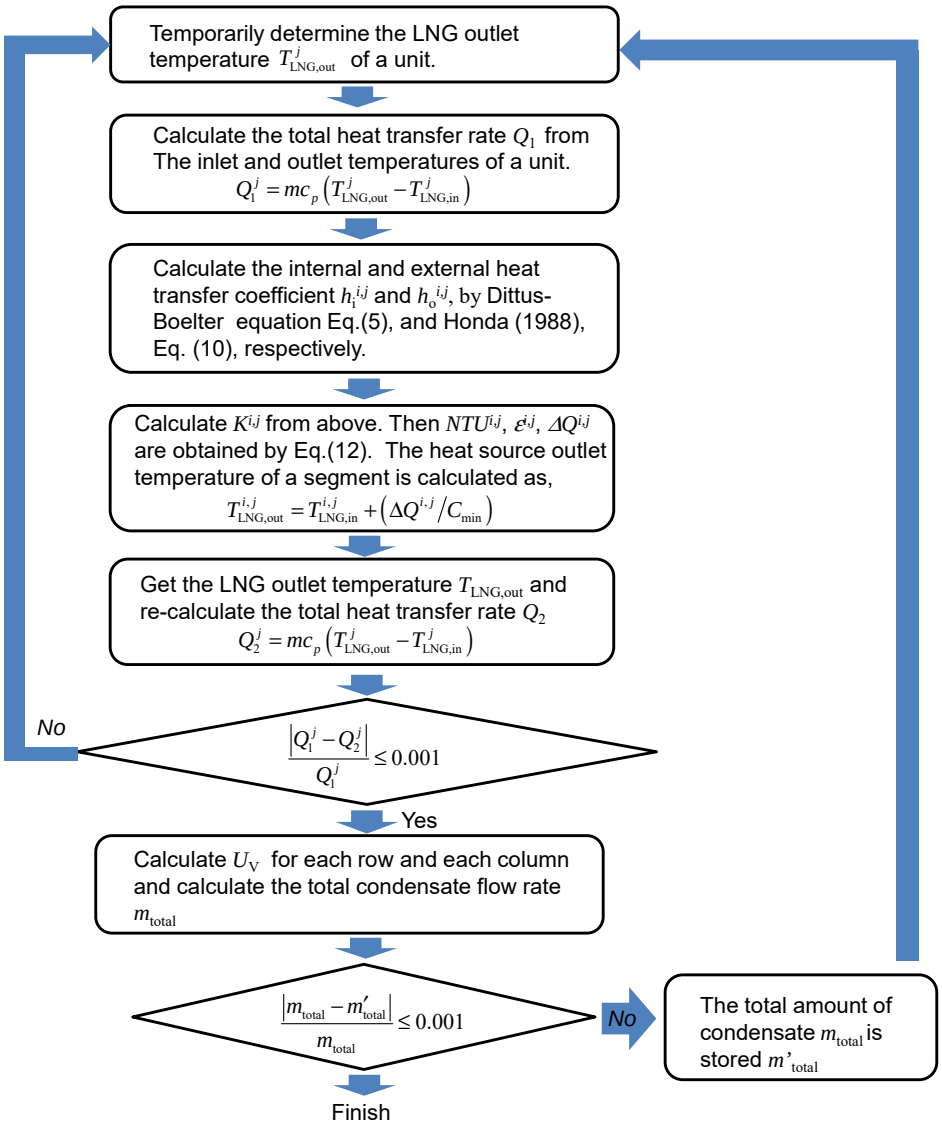

Fig. 12 Calculation procedure for condenser

4.3 Feasibility of intermediate fluids

Fig. 13 compares the heat transfer rate of each unit tube in the evaporator between selected intermediate fluids. For the comparison, the results are relatively plotted based on the heat transfer rate of propane in the first segment of second column. Along the flow direction of heat source (sea water) in tube, the heat transfer rate decreases from the upstream to the downstream as temperature difference decreases. This monotonic decrease of evaporation heat transfer qualitatively agrees with the overall heat transfer coefficient calculated by Xu et al. (2016) for propane. However, the calculation of Xu et al. (2016) does not show the heat transfer distribution in vertical direction. As shown in Fig. 13, the overall heat transfer coefficient of 1st column, i.e., the bottom tube, differs from

the other columns of 2nd to 18th. The heat transfer rate becomes higher in the second and later tubes from the bottom, because the rising bubbles induce convective contribution in the pool boiling heat transfer. This effect is more evident in the heat transfer rate of R32 and R410A, which exhibit higher pool boiling heat transfer coefficient than propane, as shown in Fig.8. Among the selected intermediate fluids, R32 shows the highest heat transfer rate. The heat transfer rate of R32 is high than that of propane approximately by 10%. While R410A shows comparable heat transfer rate to propane.

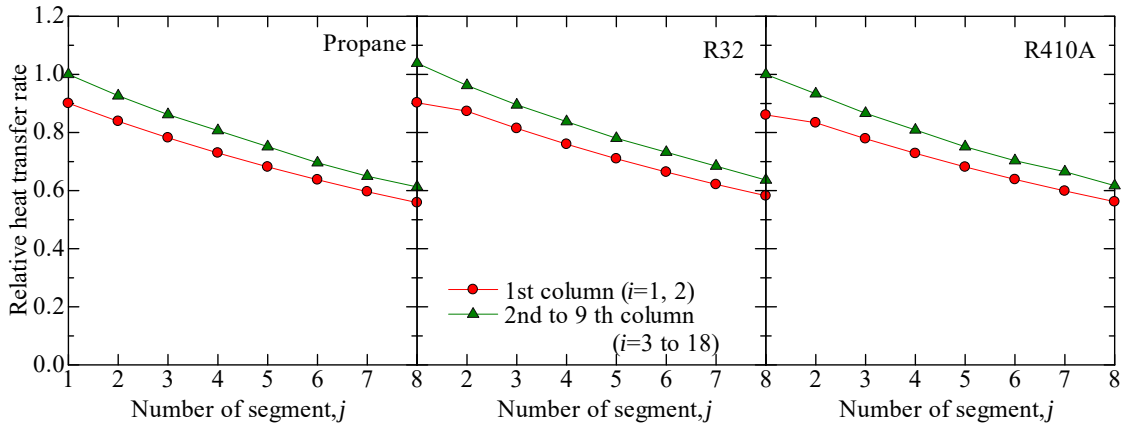

Fig. 13 Heat transfer rate profile in evaporator tube bundles predicted by Eq. (8) (Ribatski et al., 2008) and NTU method.

Fig. 14 plots the heat transfer rate of each unit tube in the condenser. A unit tube (single U tube) is divided into 26 and returns at a segment of 13th. For comparison, those results are relatively plotted based on propane. Considering the inundation, the portion of segment from 1 to 13 affected by the convective effects of dripping down liquids and drugged vapor flows. This can increase heat transfer rate and emphasize the difference between upstream and downstream. At segments from 1 to 7, the heat transfer rate decreases along the LNG flow of liquid sate with decreasing temperature difference between LNG and an intermediate fluid. More specifically, at the entrance (segments from 1 to 4), the heat transfer rate varies with the number of column. This suggests the influence of inundation is most obviously reflected in condensation heat transfer at the entrance, where higher heat transfer rate (i.e. heat flux) is exhibited from the large temperature difference. Then, at segments from 6 to 9, the heat transfer rate steeply increases. In this region, LNG flow is pseud critical region and drastically changing heat capacity and thermal conductivity results this sharp profile in heat transfer rate. Then the heat transfer rate gradually decreases to downstream. Although the local heat fluxes numerically obtained by Xu et al. (2016) do not show the effects of inundation, the overall trends are consistent to the present results on heat transfer rate distribution in condenser tube bundles. Among the selected

intermediate fluids, R32 shows the highest heat transfer rate. The heat transfer rate of R410A slightly exceeds propane.

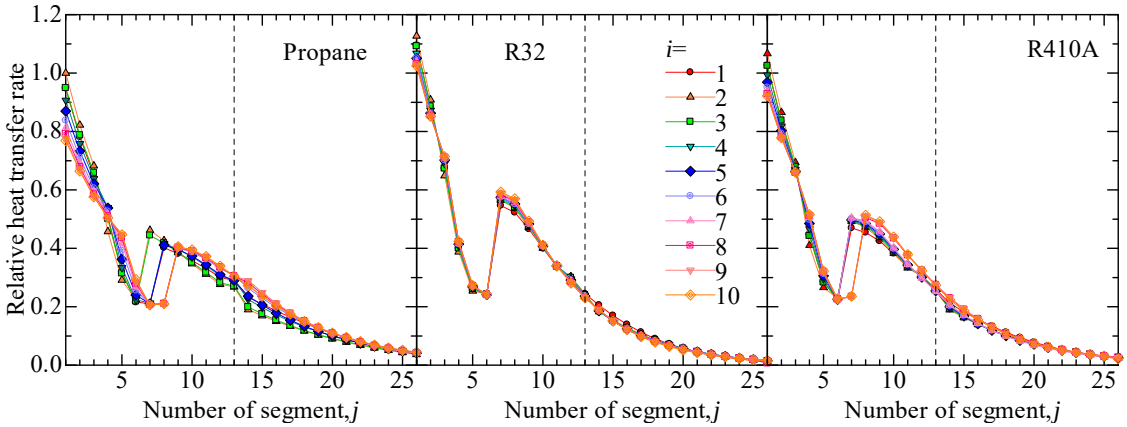

Fig. 14 Heat transfer rate profile in condenser

With respect to the total heat transfer rate in a whole tube bundle, the performance using R32 and R410 is equivalent or somewhat higher in evaporator. The total heat transfer rate in condenser is improved by 7% in R32 and by 4% in R410A compared with propane. In addition, the tube surface temperature has been checked. Although very cold LNG at a temperate of -160 °C flows into the tubes, the tube surface temperature is way above -130 °C that is higher than the freezing point of propane, R32, and R410A. Overall, the feasibility of R32 and R410A was shown as an intermediate fluid of IFV alternative to propane with respect to the heat transfer performance of the vaporizer.

5. Conclusions

In this study, the feasibility of refrigerants to intermediate fluid type vaporizer (IFV) was examined. To begin with, R32 and R410A were selected as candidate refrigerants adapting in the physical properties from the use condition of the LNG vaporizer. Next, in order to verify the applicability of the heat transfer performance of R32 and R410A which are refrigerants used in air conditioners, a boiling and condensation performance prediction models in single tubes ware developed, and the validation check with experimentally obtained heat transfer coefficients were carried out. The correlation of Jung et al. (2003) shows a qualitative tendency and that R32 and R410A may provide higher heat transfer performance than propane. Then the calculation model using ε-NTU method is developed for tube bundles in evaporator and condenser. In evaporator, the overall heat transfer coefficient of second and above column tubes increases by 10% from the bottom tube. In condenser, the effects of inundation predicted by the correlation of Honda et al. (1988) are most evident at the entrance of LNG flow and varies heat transfer rate depending the number of column. Also, the tube

bundle heat transfer model clarified that by applying R32 and R410A to IFV, the boiling performance was equivalent to that of propane, and the condensation performance was improved by about 7% in R32 and about 4% in R410A from propane. The tube surface temperature in condenser is above the freezing points of those candidate fluids. The results suggest that the application of R32 and R410A to IFV might have a higher vaporization capacity than conventional one.

ACKNOWLEDGEMENT

Professor Koyama has dedicated his life to the refrigeration sector, especially for low GWP refrigerants in the past decade. This project started in 2016. He joined the research meetings to give his ideas for the heat transfer modeling and to discuss his vision utilizing low GWP refrigerants for IFV. He was always energetic and continued research activities until his last month and left many successors in academia and industries. Here I would like to express my sincere gratitude to him.

REFERENCES

Astolfi, M., Fantolini, A.M., Valenti, G., De Rinaldis, S., Inglese, L.D., Macchi, E., 2017. Cryogenic ORC to Enhance the Efficiency of LNG Regasification Terminals. Energy Procedia 129, 42–49. https://doi.org/10.1016/j.egypro.2017.09.177

Atienza-Márquez, A., Bruno, J.C., Akisawa, A., Coronas, A., 2019. Performance analysis of a combined cold and power (CCP) system with exergy recovery from LNG-regasification. Energy 183, 448–461. https://doi.org/10.1016/j.energy.2019.06.153

Cooper, M. G., 1984. Saturation nucleate pool boiling-a simple correlation. In IChemE Symp. Ser. Vol. 86, p. 786.

DiNicola, G., Brandoni, C., DiNicola, C., Giuliani, G., 2012. Triple point measurements for alternative refrigerants. J. Therm. Anal. Calorim. 108, 627–631. https://doi.org/10.1007/s10973-011-1944-4

Dittus, F.W., Boelter, L.M.K., 1930. Heat Transfer in Automobile Radiators of the Tubular Type. Publications in Engineering, University of California, Berkeley, Vol. 2, 443.

Egashira, S., 2013. LNG vaporizer for LNG re-gasification terminal. KOBELCO Technology Review, 32, 64-69.

Gorenflo, D., Baumhögger, E., Herres, G., Kotthoff, S., 2014. Prediction methods for pool boiling heat transfer: A state-of-the-art review. Int. J. Refrig. 43, 203–226. doi:10.1016/j.ijrefrig.2013.12.012

Gorenflo, D., Baumhögger, E., Windmann, T., Herres, G., 2010. Nucleate pool boiling, film boiling and single-phase free convection at pressures up to the critical state. Part I: Integral heat transfer for horizontal copper cylinders. Int. J. Refrig. 33, 1229–1250. doi:10.1016/j.ijrefrig.2010.07.015

Hadid, Z., Zoughaib, A., 2017. Exergy recovery during LNG gasification using ambient air as heat source. Int. J. Thermodyn. 20, 36–42. https://doi.org/10.5541/ijot.5000205268

Han, H., Yan, Y., Wang, S., Li, Y.X., 2018. Thermal design optimization analysis of an intermediate fluid vaporizer for liquefied natural gas. Appl. Therm. Eng. 129, 329–337. https://doi.org/10.1016/j.applthermaleng.2017.10.043

Honda, H., Uchima, B., Nozu, S., Nakata, H., Fujii, T, 1988. Transactions of the Japan Society of Mechanical Engineers, Series B, 54 (502), 1453-1460 (in Japanese). https://doi.org/10.1016/j.ijhydene.2017.04.176

Jung, D., Kim, Y., Ko, Y., Song, K., 2003. Nucleate boiling heat transfer coefficients of pure halogenated refrigerants. Int. J. Refrig. 26, 240–248. doi:10.1016/S0140-7007(02)00040-3

Lei, X., Li, H., Zhang, Y., and Zhang, W., 2013. Effect of Buoyancy on the Mechanism of Heat Transfer Deterioration of Supercritical Water in Horizontal Tubes. ASME. J. Heat Transfer. 2013; 135(7): 071703. https://doi.org/10.1115/1.4023747

Lemmon, E.W., Huber, M. L., McLinden, M. O., Reference fluids thermodynamic and transport properties – REFPROP, NIST standard reference database 23, Version 9.2, Applied Chemicals and Materials Division National Institute of Standards and Technology Boulder, CO 80305 (2013).

Lin, W., Huang, M., Gu, A., 2017. A seawater freeze desalination prototype system utilizing LNG cold energy. Int. J. Hydrogen Energy 42, 18691–18698.

Liu, F., Dai, Y., Wei, W., Zou, J., Zhu, C., Dong, C., Hu, D., 2013. Feasibility of intermediate fluid vaporizer with spiral wound tubes. China Pet. Process. Petrochemical Technol. 15, 73–77.

McLinden, M.O., 1990. Thermodynamic properties of CFC alternatives: A survey of the available data, 13 (3), 1990, 149-162.

Myhre,G.,D. Shindell, F-.M.Br´eon,W. Collins, J. Fuglestvedt, J. Huang, D. Koch, J.F. Lamarque, D. Lee, B. Mendoza, T. Nakajima, A. Robock, G. Stephens, T. Takemura, and H. Zhan. 2013. Anthro- pogenic and Natural Radiative Forcing, in: Climate Change 2013: The Physical Science Basis. Contribution of Working Group I to the Fifth Assessment Report of the Intergovernmental Panel on Climate Change.

Nagata, R., Kondou, C., Koyama, S., 2017. Enhancement of R1234ze(Z) pool boiling heat transfer on horizontal titanium tubes for high-temperature heat pumps. Sci. Technol. Built Environ. 23, 923–932.

Nusselt, W., 1916. Die Oberflächenkondensation des Wasserdampfes. Zeitschrift des Vereines Dtsch. Ingenieure 60, 569–575.

Patel, D., Mak, J., Rivera, D., Angtuaco, J., 2013. LNG vaporizer selection based on site ambient conditions. Proceedings of the LNG, 17, 16-19.

Pu, L., Qu, Z., Bai, Y., Qi, D., Song, K., Yi, P., 2014. Thermal performance analysis of intermediate fluid vaporizer for liquefied natural gas. Applied thermal engineering, 65(1-2), 564-574.

Qi, C., Wang, W., Wang, B., Kuang, Y., Xu, J., 2016. Performance analysis of submerged combustion vaporizer. J. Nat. Gas Sci. Eng. 31, 313–319. https://doi.org/10.1016/j.jngse.2016.03.003

Reeves, L.E., Scott, G.J., Babb, S.E., 1964. Melting curves of pressure-transmitting fluids,J. Chem. Phys., 40 (12) 3662-6, 1964.

Ribatski, G., Jabardo, J.M.S., 2003. Experimental study of nucleate boiling of halocarbon refrigerants on cylindrical surfaces. Int. J. Heat Mass Transf. 46, 4439–4451. doi:10.1016/S0017-9310(03)00252-7

Ribatski, G., Saiz Jabardo, J.M., da Silva, E.F., 2008. Experimental Thermal and Fluid Science, 32, 1530–1537.

Shiralkar, B.S. and Griffith, P., 1969. Deterioration in heat transfer to fluids at supercritical pressures and high heat fluxes", Journal of Heat Transfer, Transactions of the ASME, 91 (1), 27–36.

Stephan, K., Abdelsalam, M., 1980. Heat-Transfer Correlations for Natural Convection Boiling. Int. J. Heat Mass Transf. 23, 73–87.

Sugano, K., 2006. LNG Vaporizers, Kobe Steel Engineering Reports, 56 (2), 51-55.

Xu, S., Chen, X., Fan, Z., 2016. Thermal design of intermediate fluid vaporizer for subcritical liquefied natural gas. J. Nat. Gas Sci. Eng. 32, 10–19. https://doi.org/10.1016/j.jngse.2016.04.031

Xu, S., Chen, X., Fan, Z., Chen, Y., Nie, D., Wu, Q., 2018. The influence of chemical composition of LNG on the supercritical heat transfer in an intermediate fluid vaporizer. Cryogenics, 91, 47–57. https://doi.org/10.1016/j.cryogenics.2018.01.011

Yamagata, K., Yoshida, S., Fujii, T., Hasegawa, S., Nishikawa, K, 1972. Forced Convective Heat-Transfer to Supercritical Water Flowing in Tubes, Int. J. Heat Mass Transfer, 15(12), pp. 2575–2592.

Yoshida, S., Fujii, T., Nishikawa, K., 1972. Analysis of Turbulent Forced Convection Heat Transfer to a Supercritical Fluid, Trans. JSME 38 (316), 3185-392 (in Japanese). DOI: 10.1299/kikai1938.38.3185